JOURNAL OF APPLIED ELECTROCHEMISTRY 22 (1992) 448–455

Electrochemical methods in the study of localized corrosion attack*

M. METIKOŠ-HUKOVIĆ

Institute of Electrochemistry, Faculty of Technology, University of Zagreb, Savska 16, Zagreb, Yugoslavia

I. MILOŠEV

"J. Stefan" Institute, University of Ljubljana, Jamova 39, Ljubljana, Yugoslavia

Received 16 January; revised 13 June 1991

Electrochemical methods for determining the characteristic pitting potentials of 90Cu–10Ni alloy in slightly alkaline chloride solutions are summarized and the results of measurements carried out using potentiostatic, quasi-potentiostatic, potentiodynamic and galvanostatic techniques, complemented by *ex situ* techniques – SEM and EDXA – are discussed. In borate buffer solution a passive state is established due to the formation of the oxide film with low ionic conductivity. However, in the presence of Cl^- ions, at potentials higher than a certain critical value, breakdown of the anodic passivity occurs, caused by field-stimulated chloride entry into the passive oxide film at singular point defects. The brightening of the pits formed after oxide film breakdown was established to be due to the conversion of the passivating oxide film to one of high ion conductivity. "Contaminated oxide" permits the passage of the metal cation into and through it, finally leaving it at the film/solution interface where pitting can proceed. During localized attack two characteristic potentials have to be distinguished: the potential of pit nucleation, E_n, above which pit nucleation starts, and the breakdown potential, E_b, above which the growth of nucleated pits develops. An attempt is made to compare the values of E_n and E_b obtained through different methods, and to determine the factors influencing these values in each particular method.

1. Introduction

Among the different forms of localized corrosion, pitting is encountered most often in technologically important metallic materials. Many metals and their alloys such as carbon steels, stainless steels or various Ni–, Al– and Cu– based alloys, suffer pitting in different environments, especially those containing Cl^- ions. When determining the susceptibility of metals to pitting, the critical breakdown potential serves as one of the most commonly used criteria. Breakdown of passivity and localized corrosion are of considerable practical and economic importance, as well as of theoretical interest. For practical purposes, it is desirable to determine the corrosion resistance of materials that will be exposed to various aggressive environmental conditions. A number of accelerated tests are available [1]. However, fundamental research has shown that the processes involved in pitting corrosion phenomena are generally extremely complex even under controlled laboratory conditions. The problem becomes even more complex because the exact potential at which pitting may initiate, develop or cease proved to be dependent on many variables. Different electrochemical methods are available to detect and identify pitting corrosion. they offer the best approach to providing information that would allow the interpretation of the results obtained. Furthermore, a number of environmental conditions can be studied quickly because of the rapidity with which tests can be run.

While there is plenty of data on pitting of copper [2–9], relatively little information is available concerning copper–nickel alloys. The behaviour of these alloys is presently a subject of much interest, particularly with respect to materials performance for heat exchangers in marine or power plant installations. Studies covering four main aspects have been undertaken, namely the structure and morphology of the corrosion product film [10–12], the kinetics of film formation [13–16], selective dissolution [17–22], and finally, the role of Fe content [23–25]. Investigations have been performed mainy in acid or neutral solutions. Macdonald demonstrated that the presence of sulphide in sea water induces a loss in the passivity of both 90Cu–10Ni and 70Cu–30Ni alloys [26]. It was reported recently that admiralty brass (70Cu–30Zn) suffers pitting when a poorly protective film containing Cu_2O exists on its surface [27].

Because of the lack of information concerning the behaviour of Cu–Ni alloys in alkaline media, we attempted to study the corrosion behaviour of 90Cu–10Ni alloy in slightly alkaline solutions containing chloride ions, once the metal is covered by a passive film. The possibility of correlating the characteristic

*Presented at the 11th International Corrosion Congress, Florence, Italy, April 1990

0021-891X/92

pitting potentials determined by using various electrochemical methods was of particular interest in this work. The influence of various experimental conditions such as Cl^- concentration, potential scan rate, constant current density, constant potential and time of anodization was examined.

2. Experimental details

Working electrodes were disc-shaped specimens, 1.5 cm dia., cut from sheet material. The specimen surface was abraded with SiC emery papers, finished with alumina powder down to 0.05 μm and rinsed. After placing in a Teflon holder, an area of 1 cm^2 was exposed. A carbon rod was used as the counter electrode. Potentials were measured against a saturated calomel electrode (SCE) provided with a Luggin capillary probe. The three electrodes were mounted in a PARC Corrosion Cell, Type K47.

Measurements were made in borate buffer solution, pH 9.25 (0.022 M $Na_2B_4O_7$ + 0.002 M NaOH). The influence of NaCl addition was studied in the concentration range from 0.005 to 0.5 M.

Electrochemical investigations were carried out by the following methods. (i) The potentiodynamic technique was used in two ways: (a) anodic polarization curves at slow scan rates (0.3–3 mV s^{-1}) were recorded as log current density (log i) against potential (E), after allowing the electrode to reach the open circuit potential E_{corr} for a period of 1 h; (b) cyclic voltammograms were run between the cathodic and anodic potential limits at different scan rates (0.5–50 mV s^{-1}). (ii) Galvanostatic potential transients were recorded at a constant current density from the cathodic potential −1.0 V (oxide free surface) to a certain anodic potential limit. (iii) Potentiostatic current transients were run using electrodes which were previously cathodically polarized at −1.0 V for 100 s to obtain an oxide-free surface, and then held for 300 s at the open circuit potential, E_{corr}. Finally, the current transients were monitored at a constant potential step $E_{corr} < E_t <$ a certain value more positive than the breakdown potential, E_b.

The composition and morphology of the corrosion products were examined by *ex situ* techniques. Energy dispersive X-ray analysis (EDXA) and scanning electron microscopy (SEM) were carried out using a Trakor TN-2000 energy dispersive spectrometer and a JOEL SSM-35 scanning electron microscope.

3. Results and discussion

3.1. *Linear anodic polarization: quasi-potentiostatic measurements*

Typical anodic polarization curves for a Cu–Ni electrode in borate buffer containing different NaCl concentrations are shown in Fig. 1. In the potential range examined, there are five distinct regions: the apparent Tafel region (I), the peak current region (II) of active etching, the current minimum – passive region (III),

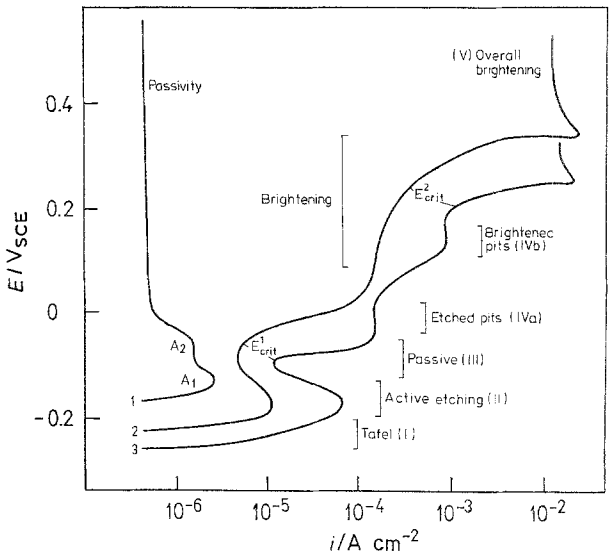

Fig. 1. Quasi-potentiostatic curves for a Cu–Ni electrode in borate buffer (1) and in borate buffer containing 0.2 M (2) and 0.5 M NaCl (3). Scan rate 0.3 mV s^{-1}.

the limiting current region – the brightening region (IV). At high chloride concentration, $Cl^- \geqslant 0.5$ M, we can distinguish the regions of etched pits (IVa) and brightened pits (IVb) and finally, the overall anodic brightening region (V) where the current density at the pit surface is nearly constant. The first feature observed as the potential increases above the open circuit potential E_{corr} is the Tafel region, (I), followed by a current peak region (II) of active etching (transition from active to passive region). The values of Taffel slopes were found to have lower values than the expected slope of 60 mV per current decade, already reported for Cu in chloride solutions [28]. A decrease of Tafel slope values is observed as the NaCl concentration increases. Cuprous species are the only electrooxidation product in this potential range, as measured using a rotating ring-disc electrode [15]. The results indicated mixed mass transfer and kinetic control with a cuprous chloride complex as the limiting diffusion species [15]. Copper electrodissolution was essentially independent of variation in H^+ concentration from 1 M up to 5 M [29]. The mechanism of Cu dissolution in chloride media (< 1 M) can be generally expressed by the two step sequence:

$$Cu + Cl^- = CuCl + e^- \quad (1)$$

$$CuCl + Cl^- = CuCl_2^- \quad (2)$$

At chloride concentrations greater than 1 M, the concentration of higher cuprous chloride complexes, such as $CuCl_3^{2-}$, becomes significant [15].

The anodic polarization curve for Cu–Ni in chloride-free borate buffer is given in Fig. 1. Two anodic peaks at −0.13 V and −0.06 V (A_1 and A_2) precede a broad passive region extending from 0 V to 0.8 V. It has already been shown that the passive film on copper [8–11] and copper–nickel alloys [30–32] is twofold, consisting of one layer growing from the original surface and an outer growing layer on the top of inner layer of thickness varying with the composition of the

electrolyte. By comparison of the current peak potential values obtained with the equilibrium potentials of Cu_2O and CuO formation [33] we can assign this behaviour to the successive formation of cuprous and cupric oxide. The electrode surface is thus covered by a protective oxide film and a passive state is established. The corresponding region in the presence of Cl^- ions is the region (III), curves 2 and 3 in Fig. 1. The increase of anodic current plateau in the passive region, as well as the narrowing of the passive range, are observable with increasing NaCl concentration. At a certain potential, E^1_{crit}, a current rise starts. However, for NaCl concentrations greater than 0.05 M (curves 2 and 3 in Fig. 1), another current plateau region appears after the current rise, denoted as the brightening region (IV). It could possibly be correlated with the formation of a certain amount of CuCl on the top of the Cu_2O layer, coinciding with the growth of the CuO layer. The important quantitative difference between the essential current density-potential relationships found for anodic passivity (see curve 1 in Fig. 1) and brightening (region IV) is in the magnitude of the limiting current density; the limiting current density may range from approximately 10^{-7} to 10^{-3} A cm^{-2} for passivity and from 10^{-2} to 1 A cm^{-2} for brightening. The subsequent anodic behaviour of the passive films depends upon the electrical characteristics of the surface layer. If its electron conductivity is low, film growth by ion transport may occur at high positive potentials. If the electron conductivity is high, electroreduction or elecrooxidation of the solution species occurs at the passive film/solution interface at a quite low anode potential. The passive film behaves like a semiconductor or insulator [34–37]. Local breakdown of passivity at a less positive potential than that required for transpassivity (the anodic oxidation of the passive film to a soluble oxide) is often induced by the presence of halide ions, of which chloride ions are the most important in practice, and the resulting local pitting is frequently rapid. It is reasonable to suggest that the thin compact solid films responsible for anodic brightening are in general not simple oxides, but are oxides "contaminated" with significant amounts of the anions from the solution [38] which permit metal cations to pass into and through it, and finally to accumulate at the film/solution interface at the same rate; the film "dissolves as fast as it forms" at quite low anode potentials [39–42].

Breakdown of the inner barrier Cu_2O layer at and above a critical breakdown potential, E^2_{crit}, see Fig. 1, curves 2 and 3, is caused by a greatly increased cation conductivity through the "contaminated" oxide film when steady state conditions have been established. According to Hoar [42], brightening is produced because crystallographic etching is suppressed by the film which dictates random removal of cations from the metal lattice on account of the random and rare arrival of film cation vacancies at the metal/film interface. At very high potentials (and high chloride concentrations) the pits formed continue to grow in extent and number until they condense and produce overall anodic brightening. The current density is constant and potential independent, as shown in Fig. 1, region (V).

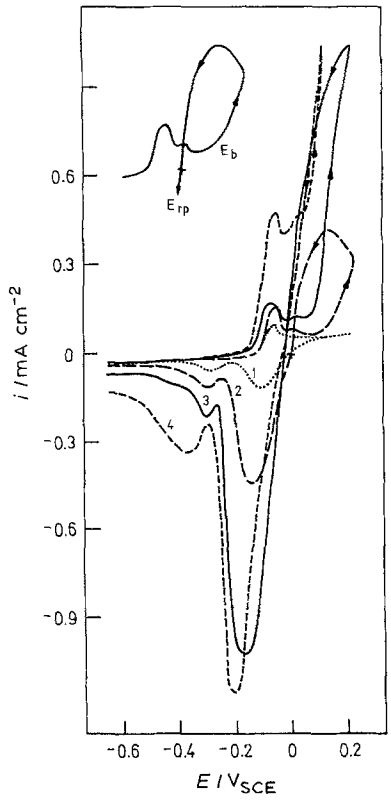

Fig. 2. Cyclic voltammograms for a Cu–Ni electrode in borate buffer containing various NaCl concentrations: (1) 0.05, (2) 0.1, (3) 0.2 and (4) 0.5 M NaCl. Scan rate 5 mV s^{-1}.

3.2. *Cyclic voltammetry measurements*

Up to this point, only processes occurring during anodic polarization were considered. In order to study both the oxidation and reduction processes on the oxide-free electrode, cyclic voltammograms starting from a limiting cathodic potential of -1.0 V were recorded. In this way, the values denoting repassivation potential, E_{rp}, and breakdown potential, E_b, could also be obtained.

Figure 2 shows the influence of NaCl concentration in the solution. The potential range examined is limited by the anodic potential limit $E = 0.12$ V. In chloride-free borate buffer solution, curve 1 in Fig. 1, a double anodic peak appears, splitting into two well defined cathodic peaks upon potential scan reversal. This behaviour is consistent with the formation of a duplex passive film. Its solid state reduction takes place in two stages, namely an outer CuO layer reduces to Cu_2O and an inner Cu_2O layer to pure copper metal [32]. Addition of NaCl to the solution results in the better separation of the anodic peaks, and the first anodic peak corresponding to the Cu(I) oxide now predominates, Fig. 2. The area under the first anodic peak increases proportionally to the NaCl concentration, and such behaviour can be linked to an increasing amount of cuprous soluble species in the vicinity of

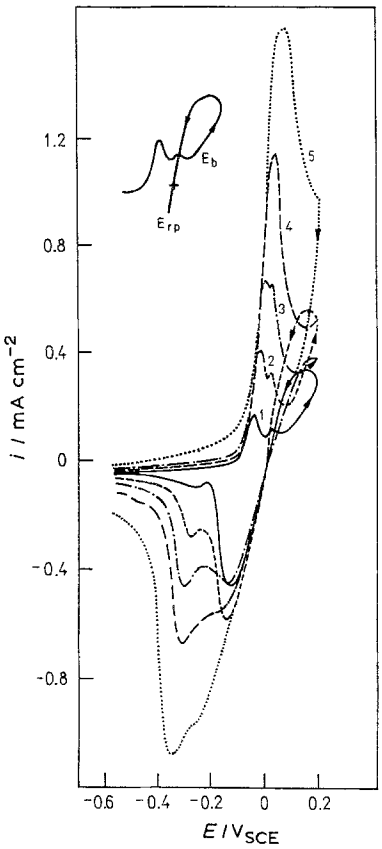

Fig. 3. Cyclic voltammograms for a Cu–Ni electrode in borate buffer containing 0.1 M NaCl, obtained using different scan rates: (1) 1, (2) 5, (3) 10 and (4) 20 mV s^{-1}.

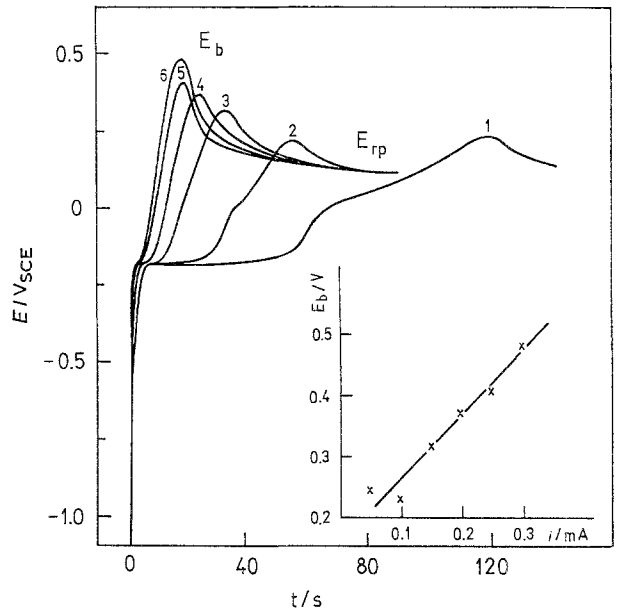

Fig. 4. Galvanostatic charging curves for a Cu–Ni electrode in borate buffer containing 0.1 M NaCl recorded at various constant current densities: (1) 0.05, (2) 0.1, (3) 0.15, (4) 0.2, (5) 0.25 and (6) 0.3 mA cm^{-2}. Detail showing the breakdown potential, E_b against current density plot.

the electrode surface [28]. Current rise starts at the breakdown potential, E_b, continuing even after the potential scan reversal. The hysteresis loop thus obtained allows the repassivation (nucleation) potentials, E_{rp} (E_n), to be determined [43]. Within the potential range examined, Fig. 2, the breakdown potential, E_b, is not reached unless the NaCl concentration is greater than 0.05 M. Repassivation potentials correspond to the potential values below which no pitting occurs and above which pit nucleation begins. Increasing the NaCl concentration produce a more pronounced hysteresis loop and causes a shift of the corresponding breakdown potential toward more negative values. Consequently, the difference between E_{rp} and E_b is smaller.

Figure 3 indicates the importance of the appropriate choice of scan rate when determining the breakdown potentials. The voltammograms were recorded in a borate buffer solution containing 0.1 M NaCl. While the slow scan cycle yields two anodic peaks followed by the onset of passivity, the sharp current increase associated with the localized attack and a hysteresis loop after potential scan reversal, when using a rapid scan rate, results in a single anodic peak and does not show the loop at all. This behaviour suggests that in the presence of Cl^-, besides the potential, the time of anodization also plays an important role in determining the breakdown potential. It will be shown below that the more noble the potential, the shorter the incubation time for breakdown of the oxide film, which leads to pit growth or general corrosion. Consequently, when the potential scan rate is high, a rapid current increase can be observed only at more noble potentials, corresponding to a sufficiently short pit incubation time.

3.3. *Measurements of the potential/time transients at a constant current density*

Figure 4 shows potential/time transients for a Cu–Ni electrode in borate buffer containing 0.1 M NaCl. When a current density higher than the critical current for passivation is applied to the oxide-free surface, the anode potential increases rapidly with time due to alloy dissolution. The potential arrest is eventually reached at −0.18 V as a consequence of oxide film formation. For transients recorded at lower current densities, another potential arrest appears at approximately 0.05 V, confirming the formation of the CuO layer. The region of almost linear increase of anodic potential which follows is mainly due to the growth of the oxide film. In a chloride-free solution, the region of linear potential increase extends up to approximately 0.8 V, and can be correlated to the passive region in quasi-potentiostatic curves, see curve 1 in Fig. 1. In chloride containing solutions, the potential rise, i.e., the passivation rate, is slowed down, and furthermore, a potential maximum appears at a certain potential. This maximum is thought to correspond to the breakdown potential, E_b, the appearance of which is the consequence of competition between two processes, namely, further oxide film growth and its breakdown. After prevalence of the latter reaction at E_b, the potential drops to a steady value, corresponding to the repassivation potential, E_{rp}. Under galvanostatic conditions, it is the only potential at

Table 1. Correlation between breakdown potential values determined by the quasi-potentiostatic and galvanostatic methods. E_b^* — potential value at which the current density of 0.2 mA cm^{-2} is reached, evaluated from curves presented in Fig. 1; E_b^{**} — value of potential maximum of E/t curve, at a constant current density of 0.2 mA cm^{-2}, Fig. 4

c_{NaCl}	E_b^*/V	E_b^{**}/V
0.05	0.49	0.52
0.10	0.25	0.24
0.20	0.12	0.10
0.50	0.04	0.03

which the active area remains constant and independent of time [43]. The values of maximum E_b are dependent upon the constant current density applied, see detail in Fig. 4, according to the following relation:

$$E_b = a + bi \quad (3)$$

The repassivation potentials, E_{rp} are, however, unaffected by the current density applied, reaching almost identical values after the potential drop.

Table 1 is given in order to correlate the breadown potential values determined by quasi-potentiostatic and galvanostatic measurements. As a reference value, the potential at which the current density reaches the value of 0.2 mA cm^{-2}, E_b^*, and the value of the potential maximum at constant current density of 0.2 mA cm^{-2}, E_b^{**}, were chosen for quasi-potentiostatic and galvanostatic experiments, respectively, see Figs 1 and 4. The results obtained are comparable, which confirms that the potential maximum on the potential/time curve could be identified as a breakdown potential. However, when comparing the results with those obtained by some other method, the dependence upon the value of the constant current density should be considered, see detail in Fig. 4.

3.4. *Measurements of current/time transients at a constant potential*

Current/time transients obtained by changing the potential gradually at a constant rate and recording the current-time relationships at each assigned potential, E_t, are shown in Figs 5 and 6. Curves recorded at the same potentials in chloride-free borate buffer are given in detail. In the absence of NaCl, the current decreases monotonically to reach the corresponding steady passive state, where electronic conductivity prevails. Similar behaviour is obtained in the presence of NaCl when the constant potential E_t is more negative than a certain critical potential, E_n, Fig. 5. However, the anodic currents are much higher in the presence of Cl^- ions as a result of the hindered formation of oxide film. At potentials close to E_n, Fig. 6, the current initially decreases to a minimum value, yielding the corresponding characteristic pitting time parameter, namely the incubation time, t_i. A steady current rise starts later. Such behaviour can be explained through continual competition between film repassivation and localized breakdown, the latter gradually becoming the dominant factor. The dehydrated Cl^- ion adsorbed on the oxide film/electrolyte interface begins to enter and penetrate the oxide film at singular point defects of less perfection [44]. Thus, the incubation time, t_i, for initiation of passivity breakdown, i.e., for pit nucleation after Cl^- has been introduced into an oxide film held at or just above the pit nucleation potential, E_n, is caused by the time required for Cl^- penetration into the outer CuO layer of the duplex film [45]. Since an oxide containing foreign anions ("contaminated") is a much better ionic conductor than the original passive oxide, it may be able to release the Cu(I) cations rapidly at the film/solution interface so that consequent pitting can proceed.

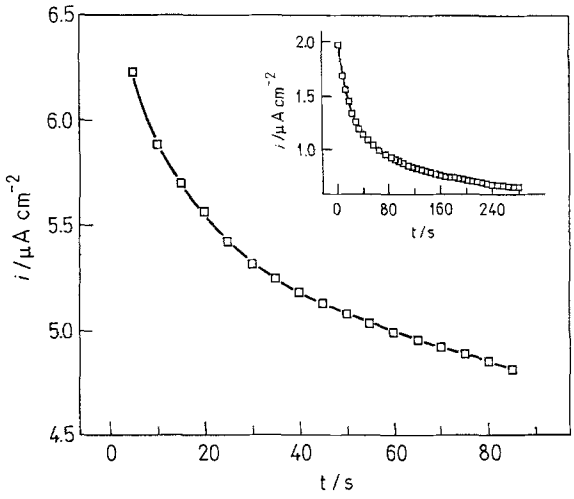

Fig. 5. Current transients recorded at constant potential E_t = 0.05 V for a Cu–Ni electrode in borate buffer (detail) and in borate buffer containing 0.1 M NaCl.

The relationship between the constant potential E_t and the rate of Cl^- penetration, defined as $1/t$, is shown in Fig. 7. The following equation is fulfilled:

$$1/t = a' + b'E_t \quad (4)$$

where a' and b' are constants and t is the period of time after which the current rise starts. The rate of Cl^- penetration initially rises steadily with potential and the constant b' has a value of approximately 0.1.

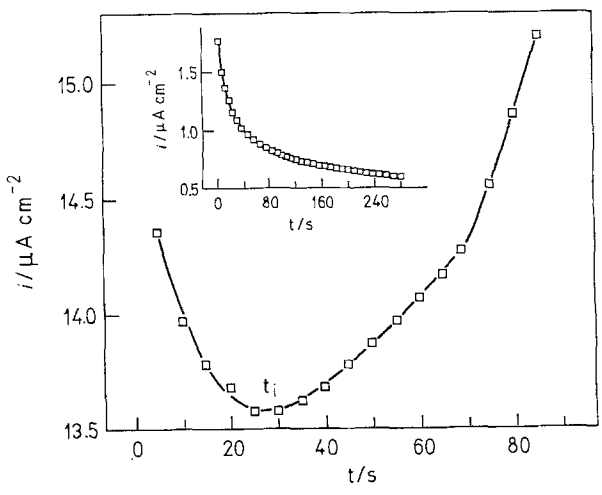

Fig. 6. Current transients recorded at constant potential E_t = 0.15 V for Cu–Ni electrode in borate buffer (detail) and in borate buffer containing 0.1 M NaCl.

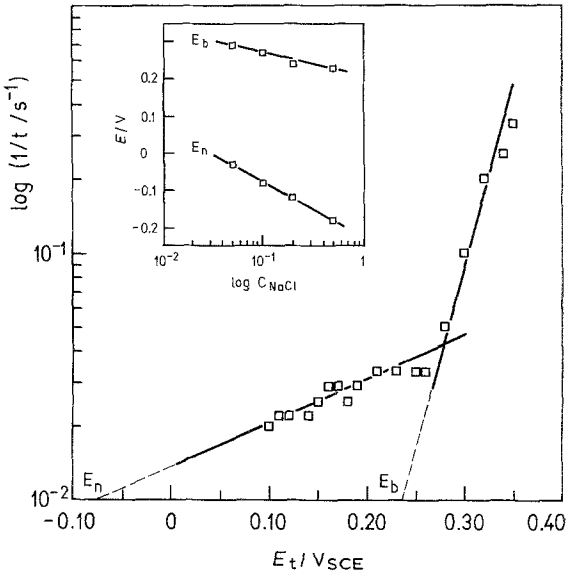

Fig. 7. Rate of Cl^- penetration log $(1/t)$ as a function of the constant potential, E_t for a Cu–Ni electrode in borate buffer containing 0.1 M NaCl. Detail showing the dependence of the extrapolated values, E_n and E_b, upon NaCl concentration.

However, as the potential E_t is made more positive, the breakdown rate becomes progressively higher, and the value of b' changes to 3.9. Two straight lines of different slopes are obtained, Fig. 7. Extrapolation of each of these straight lines to infinite time gives the exact values of the critical pitting potentials: the potential of pit nucleaction, E_n, and the breakdown potential, E_b. In this way, two defined potential regions are obtained: the region of pit nucleation between the E_n and E_b, and the region of pit growth at potentials more positive than E_b. The extrapolated values of E_n and E_b move toward more negative potentials with increasing NaCl concentration, see detail in Fig. 7. The following equation is fulfilled:

$$E_n, E_b = a'' + b'' \log c_{NaCl} \quad (5)$$

where a'' and b'' are constants, b'' is $-0.14\,V^{-1}$ for the E_n and $-0.07\,V^{-1}$ for the E_b.

For a constant potential E_t close to E_b, the transition from the period of pit nucleation to that of pit growth can be recognized in the current/time plot as the change of the current rise slope at the inflection point, denoted as the induction time, τ. By representing the current-time relationships in logarithmic form, this point is seen more clearly, Fig. 8. In this way, more accurate values of the induction times, τ, could be obtained. Thus, the period between the incubation time, t_i, and induction time, τ, corresponding to the period of pit nucleation, is characterized by a small, but measurable, increase with time. The apparent pitting current density $(i_c - i_p)$ against time $(t - t_i)$ plot in Fig. 8 fits the Engell-Stolica equation, [46]:

$$(i_c - i_p) = k(t - t_i)^b \quad (6)$$

where i_c and i_p are the corrosion and passive current densities, respectively, t is the total time, t_i is the incubation time, and k and b are constants. The slope of the first straight line, corresponding to pit nucleation, is $b_1 = 0.33$, but changes to $b_2 = 1.96$ after τ is

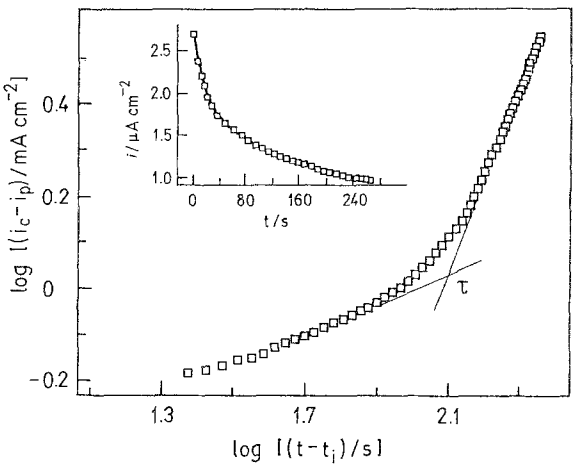

Fig. 8. log $(i_c - i_p)$ against log $(t - t_i)$ plot evaluated from the current transients recorded at constant potential $E_t = 0.2$ V for a Cu–Ni electrode in borate buffer containing 0.1 M NaCl. Detail showing the current transient obtained at the same potential in chloride-free solution.

exceeded, thus indicating the development of steady pit growth [43, 46].

At constant potential E_t, the value of b_2 is dependent upon NaCl concentration. An increase of NaCl concentration to 0.5 M causes a change in the value of b_2 to 2.63, Fig. 9, revealing that the number of pits increases with time [43].

In order to check the critical pitting potentials obtained using potentiostatic transients, a comparison with the critical potentials evaluated from the quasi-potentiostatic curves in Fig. 1, was made. The potential of pit nucleation, E_n, is defined as the potential below which no pitting occurs, and above which pit nucleation begins. Consequently, it can be correlated with the potential E^1_{crit} at which the sudden current increase within the passive range takes place. However, it has to be emphasized that only the values obtained using very slow scan rate can te taken for such a correlation. The polarization curves obtained using a high scan rate do not show such detailed structure and, usually, only the critical pitting potential, E^2_{crit}, can be recognized. Satisfactory agreement was found between the breakdown potentials, E_b and critical potentials E^2_{crit}, Table 2.

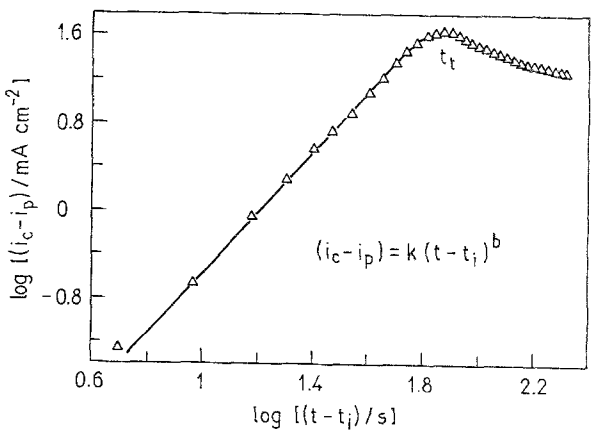

Fig. 9. log $(i_c - i_p)$ against log $(t - t_i)$ plot evaluated from the current transients recorded at constant potential $E_t = 0.2$ V for a Cu–Ni electrode in borate buffer containing 0.5 M NaCl.

Table 2. Correlation between potential of pit nucleation, E_n and breakdown potential, E_b, evaluated from $1/t_i$ against E_t plots, Fig. 7, and E^1_{crit} and E^2_{crit} determined from quasi-potentiostatic curves, Fig. 1

c_{NaCl}/M	E_n/V	E^1_{crit}/V	E_b/V	E^2_{crit}/V
0.1	−0.08	−0.05	0.27	0.27
0.2	−0.12	−0.08	0.24	0.20
0.5	−0.18	−0.10	0.23	0.19

The transition from the passive region (III) to the etched pits region (IVa) is represented by the current transient in Fig. 6. Figures 8 and 9 show the current transients for transition from the passive region (III) to brightened pits region (IVb). Since in the latter case the Cl^- concentration in the solution is high, the value of induction time τ is very short and pit growth develops almost immediately. However, after this sharp increase the current reaches a maximum, having values up to 50 mA cm^{-2}, and finally decreases very slowly, although it is still very large. In logarithmic form, such a maximum appears at the transition time, t_t, where an inflection between the two stages occurs, Fig. 9. The current maximum observed at the transition point is related to the first appearance of blue-green spots of $Cu_2(OH)_3Cl$ at the electrode surface, which precipitate very rapidly. The second current plateau decrease which then follows is related to the complete coverage of the electrode surface by a large amount of precipitated product as shown in Fig. 10a. A further insight into the processes occurring at a Cu–Ni electrode in chloride solutions was enabled by SEM observations and EDXA data. The SEM micrograph of the electrode surface, after an anodic cycle in borate buffer containing 0.05 M NaCl, revealed the presence of holes in the zone of attack, filled with a whitish orange corrosion product. The EDXA signals of this product correspond to the presence of a CuCl layer, Fig. 10b. However, an increase of NaCl concentration to 0.5 M results in the appearance of an additional product, Fig. 10a. A thick blue-green layer forms, which is very poorly adherent and obviously precipitates from solution. Large crystals form very rapidly, completely covering the electrode surface and even accumulating at the bottom of the cell. The attacked surface, covered by randomly distributed holes, could be seen only after removing this outer non-adherent layer. This behaviour is consistent with that already observed in the anodic polarization curves, Fig. 1, as a secondary current limiting region. The electrode surface under progressive pitting thus becomes covered by a thick layer of precipitated $Cu_2(OH)_3Cl$, which acts as a barrier to separate the pit interior from the bulk solution and contributes, in a way, to process stabilization. Nevertheless, current values are still very high, as a consequence of the previous enhanced dissolution. The improvement of the brightening at high anode potentials is caused by better maintenance of the compact solid film in contact with the metal/film interface by the higher field.

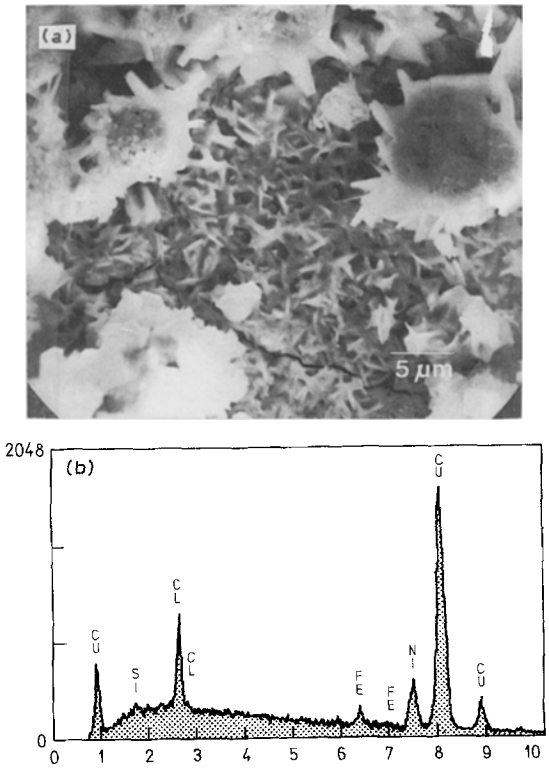

Fig. 10. (a) SEM micrograph showing large crystals of the precipitated product, obtained after an anodic cycle in borate buffer containing 0.5 M NaCl and (b) EDXA spectrum of the precipitated product.

4. Conclusions

Investigations of pitting corrosion phenomena on Cu–Ni alloy were performed through several electrochemical methods. Results obtained by potentiodynamic, galvanostatic and potentiostatic modes revealed that actually two characteristic time parameters (incubation time, t_i, and induction time, τ) and two characteristic potentials (critical potential of pit nucleation, E_n, and breakdown potential, E_b) can be recognized during duplex passive film breakdown. It is necessary to distinguish which one of these potentials is being measured by a particular method.

Analysis of the current/time transients recorded at a constant potential allows the determination of both characteristic pitting potentials, E_n and E_b, Fig. 7. These potentials clearly divide the regions where pit nucleation occurs from that where pit growth is possible. E_n is denoted as the potential below no pitting occurs, and above which pit nucleation starts. In that sense, it can be regarded as the protection or repassivation potential, E_{rp}, which can be determined from the potential/time transients, Fig. 4, or from potentiodynamic measurements after the anodic scan reversal, Figs 2, 3. During linear anodic polarization pit nucleation can actually start before the sudden current rise is observed at E_b, but continual change of potential with time does not allow this change to be recognized. Consequently, the potentiodynamic method is not recommended for detailed examination of the pitting process unless a very slow scan rate is used, as in Fig. 1. From the anodic polarization curves

recorded using 0.3 mV s^{-1} both critical pitting potentials could be distinguished. The values of E^1_{crit} and E^2_{crit}, representing the potential of pit nucleation and the breakdown potential, respectively, compare well with the corresponding critical pitting potentials obtained through the other methods used, Tables 1 and 2.

The indubation time t_i, for initiation of passivity breakdown, i.e., for a first pit nucleation is caused by the time required for Cl^- penetration into the outer CuO layer of the duplex passive film.

Breakdown of the inner barrier Cu_2O layer at and above critical anode breakdown potential, E_b, is caused by a greatly increased cation conductivity through the "contaminated" oxide film when steady state conditions have been established during the induction time, τ. The breakdown potential, E_b, can be recognized relatively easily by each of the methods used: (i) from current/time transients as the extrapolated value in the $1/t$ against E_t plots (where t is infinite); (ii) from quasi-potentiostatic measurements as the potential within the brightening range at which the current abruptly starts to rise, Fig. 1; (iii) from potential/time measurements as the potential maximum, the appearance of which is the consequence of competition between two processes, namely, further oxide film growth and its breakdown, Fig. 4.

However, the limitation of individual methods should be considered in order to achieve exact results, or to compare the values determined through different methods. Cyclic voltammetry measurements and measurements performed at a constant current density allow the determination of both critical parameters, the repassivation potential, E_{rp}, and the breakdown potential, E_b. E_b values are, however, strongly dependent upon the constant current density applied, as a consequence of the different passivation and pit nucleation rates thus taking place, Fig. 4. On the other hand, E_b values are dependent on the potential scan rate: the higher the scan rate, the more positive E_b values become, Fig. 3. When the potential scan rate is high, a rapid current increase can be observed only at potentials corresponding to a sufficiently short incubation time. Therefore, E_b values will be overestimated.

It was shown that the current/time transients recorded under a constant potential step could be successfully used for kinetic studies of passive film breakdown, thus enabling the different stages involved in an overall process to be recognized. Nevertheless, the reproducibility of the results obtained can still be poor. For that reason, the conditions of the passive film formation and its growth should be controlled in order to obtain the exact correlation between the critical pitting parameters and the properties of the passive film itself. A new passive film should be used for each constant potential being measured. In that way, the characteristic pitting parameters could be measured as a function of each particular property of the passive film, which could affect its susceptibility towards localized breakdown, e.g., passive film thickness or potential and time of anodic pretreatment [32, 45].

References

[1] G. S. Haynes and R. Baboian (Eds.) 'Laboratory Corrosion Tests and Standards', ASTM, STP 866, Symposium by ASTM Committee 6-1 on Corrosion of Metals, Bal Harbour, FL (1983).
[2] H. S. Campbell, *J. Inst. Metals* **77** (1950) 345.
[3] V. F. Lacey, *Br. Corros. J.* **2** (1967) 175.
[4] M. Pourbaix, *Werkst. Korros.* **20** (1969) 772.
[5] Z. Szklarska-Smialowska, *Corrosion* **27** (1971) 223.
[6] R. Retief, *Br. Corros. J.* **8** (1973) 265.
[7] E. Mattson, *ibid.* **15** (1980) 6.
[8] D. Vasquez Moll, M. R. G. de Chialvo, R. C. Salvarezza and A. J. Arvia, *Electrochim. Acta* **30** (1985) 1011.
[9] M. Drogowska, L. Brossard and H. Menard, *Corrosion* **43** (1987) 549.
[10] R. F. North and M. J. Pryor, *Corros. Sci.* **10** (1970) 297.
[11] C. Kato, J. E. Castle, B. G. Ateya and H. W. Pickering, *J. Electrochem. Soc.* **127** (1980) 1897.
[12] F. J. Kuijers and V. Ponec, *Surface Sci.* **68** (1977) 294.
[13] H. P. Dhar, R. E. White, G. Burnell, L. R. Cornwell, R. B. Griffin and R. Darby, *Corrosion* **41** (1985) 317.
[14] C. Kato, B. G. Ateya, J. E. Castle and H. W. Pickering, *J. Electrochem. Soc.* **127** (1980) 1890.
[15] H. P. Lee and Ken Nobe, *ibid.* **131** (1984) 1236.
[16] M. E. Walton and P. A. Brook, *Corros. Sci.* **17** (1977) 317.
[17] E. D. Verink Jr, and R. H. Heidersbach Jr, in 'Localized Corrosion – Cause of Metal Failure', ASTM STP **516** (1972) 303.
[18] W. B. Brooks, *Corrosion* **24** (1968) 1711.
[19] R. G. Blundy and M. J. Pryor, *Corros. Sci.* **12** (1972) 65.
[20] K. D. Efird, *Corrosion* **31** (1975) 77.
[21] A. M. Beccaria and J. Crousier, *Br. Corros. J.* **24** (1989) 49.
[22] E. D. Verink and M. Pourbaix, *Corrosion* **27** (1971) 492.
[23] J. M. Popplewell, R. J. Hart and J. A. Ford, *Corros. Sci.* **13** (1973) 295.
[24] R. Gasparini, C. Della Rocca and E. Ioannilli, *ibid.* **10** (1970) 157.
[25] R. F. North and M. J. Pryor, *ibid.* **8** (1968) 149.
[26] D. D. Macdonald, B. C. Syrett and S. S. Wing, *Corrosion* **35** (1979) 367.
[27] Z. Xia and Z. Szklarska-Smialowska, *ibid.* **46** (1990) 85.
[28] C. Deslouis, B. Tribollet, G. Mengoli, M. M. Musiani, *J. Appl. Electrochem.* **18** (1988) 374.
[29] H. P. Lee and Ken Nobe, *J. Electrochem. Soc.* **132** (1985) 1031; **133** (1986) 374.
[30] J. Kruger, *ibid.* **106** (1959) 847; **108** (1961) 503.
[31] H. Leidheiser, in 'The Corrosion of Copper, Tin and their Alloys', John Wiley & Sons, New York (1971) p.28.
[32] I. Milošev and M. Metikoš-Huković, *J. Electrochem. Soc.* **138** (1991) 61.
[33] U. Bertocci and D. D. Wagman, in 'Standard Potentials in Aqueous Solution' (edited by A. J. Bard, R. Parsons and J. Jordan), Marcel Dekker, New York (1985) p. 287.
[34] U. Stimming, *Electrochim. Acta* **31** (1986) 415.
[35] K. E. Heusler and K. Suk Yun, *ibid.* **22** (1977) 977.
[36] M. Metikoš-Huković and B. Lovreček, *ibid.* **25** (1980) 717.
[37] M. Metikoš-Huković, *ibid.* **26** (1981) 989.
[38] B. MacDougall and M. Cohen, *J. Electrochem. Soc.* **124** (1977) 1185.
[39] T. P. Hoar, in 'Modern Aspects of Electrochemistry', No. 2 (edited by J. O'M. Bockris), Butterworths, London, (1959) p. 262.
[40] T. P. Hoar and J. A. S. Mowat, *Nature* **165** (1950) 64.
[41] N. D. Tomashov, G. P. Chernova and O. N. Markova, *Corrosion* **19** (1964) 1667.
[42] T. P. Hoar, *Corros. Sci.* **7** (1967) 341.
[43] Z. Szklarska-Smialowska, in 'Pitting Corrosion of Metals', NACE, Houston, TX (1986).
[44] B. MacDougall, D. F. Mitchell and M. J. Graham, *Corrosion* **38** (1982) 85.
[45] I. Milošev and M. Metikoš-Huković, *Corrosion*, in press.
[46] H. J. Engell and N. D. Stolica, *Z. Phys. Chem. Neue Folge* **20** (1959) 113.